nature physics

ARTICLES

PUBLISHED ONLINE: 10 JANUARY 2012 | DOI: 10.1038/NPHYS2179

Acceleration in the linear non-scaling fixed-field alternating-gradient accelerator EMMA

S. Machida[1]*, R. Barlow[2], J. S. Berg[3], N. Bliss[4], R. K. Buckley[4,5], J. A. Clarke[4,5], M. K. Craddock[6,7], R. D'Arcy[8], R. Edgecock[1,2], J. M. Garland[5,9], Y. Giboudot[5,10], P. Goudket[4,5], S. Griffiths[4,11], C. Hill[4], S. F. Hill[4,5], K. M. Hock[5,12], D. J. Holder[5,12], M. G. Ibison[5,12], F. Jackson[4,5], S. P. Jamison[4,5], C. Johnstone[13], J. K. Jones[4,5], L. B. Jones[4,5], A. Kalinin[4,5], E. Keil[14], D. J. Kelliher[1], I. W. Kirkman[5,12], S. Koscielniak[6], K. Marinov[4,5], N. Marks[4,5,12], B. Martlew[4], P. A. McIntosh[4,5], J. W. McKenzie[4,5], F. Méot[3], K. J. Middleman[4,5], A. Moss[4,5], B. D. Muratori[4,5], J. Orrett[4,5], H. L. Owen[5,9], J. Pasternak[1,15], K. J. Peach[16], M. W. Poole[4,5], Y-N. Rao[6], Y. Saveliev[4,5], D. J. Scott[4,5,13], S. L. Sheehy[1,16], B. J. A. Shepherd[4,5], R. Smith[4,5], S. L. Smith[4,5], D. Trbojevic[3], S. Tzenov[17], T. Weston[4], A. Wheelhouse[4,5], P. H. Williams[4,5], A. Wolski[5,12] and T. Yokoi[16]

In a fixed-field alternating-gradient (FFAG) accelerator, eliminating pulsed magnet operation permits rapid acceleration to synchrotron energies, but with a much higher beam-pulse repetition rate. Conceived in the 1950s, FFAGs are enjoying renewed interest, fuelled by the need to rapidly accelerate unstable muons for future high-energy physics colliders. Until now a 'scaling' principle has been applied to avoid beam blow-up and loss. Removing this restriction produces a new breed of FFAG, a non-scaling variant, allowing powerful advances in machine characteristics. We report on the first non-scaling FFAG, in which orbits are compacted to within 10 mm in radius over an electron momentum range of 12–18 MeV/c. In this strictly linear-gradient FFAG, unstable beam regions are crossed, but acceleration via a novel serpentine channel is so rapid that no significant beam disruption is observed. This result has significant implications for future particle accelerators, particularly muon and high-intensity proton accelerators.

The fixed-field alternating-gradient (FFAG) accelerator, proposed independently by Ohkawa, Kolomensky and Symon in the early 1950s, employs an annular ring of magnets with alternating field gradients; Symon *et al.*[1] review the orbit dynamics of the various designs. The creation of strong focusing from the gradients and edges of these magnets allows GeV energies to be reached without ramping the magnetic field, permitting higher repetition rates and beam intensities than in synchrotrons. Scaling FFAGs are accelerators in which the transverse 'betatron' focusing seen by the particle bunches is kept constant during acceleration by using the same magnet shape and field index at all radii. Selecting a suitable (and constant) advance in betatron phase per turn (conventionally measured by the 'tune' or number of oscillations) avoids the resonant accumulation of errors and gives stable transverse motion. Several electron models were successfully built between 1956 and 1961 (ref. 2).

In recent years there has been renewed interest in FFAGs as a means of rapid acceleration of unstable muons for high-energy physics[3–5]; as a compact but flexible source for charged particle therapy[6,7]; as a high-reliability, compact proton driver of neutron or muon production for neutron- or muon-based physics[8], and for accelerator-driven reactor systems[9]. Several scaling proton FFAGs have now been constructed[9,10], demonstrating proton acceleration with fast sweeping radiofrequency, but in common with all scaling designs the magnets and radiofrequency cavities are relatively large and complex.

Mills[11] and Johnstone[12] suggested that if acceleration is rapid enough, then the effects of allowing the phase advance per turn to change and pass through a resonance condition might be tolerable, thus removing the restrictive scaling requirement; Machida and Kelliher[13] subsequently showed in simulations that this is indeed the case: the orbit and optics distortion is excited by random dipole and quadrupole kicks rather than periodic resonance. The field variation with radius may then be simplified; in the most extreme case reduced to a simple linear gradient[14]. The linear gradient can be chosen such that acceleration over a given energy range can occur within a far smaller range of orbital radii, thereby allowing much more compact magnets. The decreased variation in orbital circumference and orbital period at relativistic energies allows operation with fixed rather than swept-frequency accelerating cavities, permitting continuous-wave, instead of pulsed beam acceleration. The beam can be induced to gain energy by following novel 'serpentine' paths in longitudinal phase space, which are outside the bucket of stable motion employed in standard-design synchrotrons and scaling FFAGs (refs 15–21).

To confirm that (1) the scaling requirement may be safely removed[22], and (2) serpentine acceleration is both feasible and practical, an experimental investigation was required. This paper reports the first experimental demonstration of the non-scaling FFAG principle using the Electron Model for Many Applications, EMMA (refs 23,24)—a 10–20 MeV linear non-scaling FFAG constructed at the Daresbury Laboratory in the UK.

A full list of affiliations appears at the end of the paper.

Table 1 | Principal parameters of EMMA.

Momentum	10.5–20.5 MeV/c
Circumference	16.57 m
Number of cells	42
Focusing	Focusing/defocusing quadrupole doublet
Nominal integrated quadrupole gradient (focusing quadrupole/defocusing quadrupole)	0.402/−0.367 T
Radiofrequency	1.301 GHz
Number of radiofrequency cavities	19
Tune shift for the momentum range above	∼0.3 to ∼0.1 cell^{-1} (∼12- to ∼4-ring)
Acceptance (normalized)	3π mm rad

One of the principal applications for non-scaling FFAGs is the acceleration of muons in a neutrino factory or muon collider. EMMA has therefore been designed to dynamically mimic such a FFAG using electrons, which are easier to produce and accelerate. Because of the muon's short lifetime of 2.2 μs in the rest frame, acceleration would have to be completed within around ten turns in either application, so by analogy a total voltage of more than 1 MV per turn is required in EMMA, provided by nineteen single-cell normal-conducting cavities[25].

The magnet lattice consists of forty-two identical cells containing quadrupole doublets[26]. The focusing and defocusing quadrupoles are offset horizontally from the beam axis to provide a net bending force and thereby circulate the beam around the machine. Over the chosen acceleration range of 10.5–20.5 MeV/c, the fixed field and absence of nonlinear elements for chromaticity correction causes the tune to vary from typically 0.3 cell^{-1} to 0.1 cell^{-1}, or 12-ring to 4-ring, in both the horizontal and vertical planes. A number of integer tunes of the ring—potential sites for instability—are naturally crossed. Table 1 lists the principal EMMA parameters.

Two important aims of the present experiment are to measure the beam position and orbital period as a function of momentum. Beam position monitors (BPMs) are used to detect the beam centroid position for each passage of the beam, so that both the betatron oscillations and the closed orbit distortion (COD) can be measured[27].

The ALICE (Accelerators and Lasers In Combined Experiments) accelerator[28] is used as an electron source and a single 40 pC bunch is injected into EMMA. A more detailed description of injection as well as extraction can be found in refs 29,30. For all measurements reported here, the momentum of the beam provided by the ALICE injector was fixed at 12.5 MeV/c. To characterize EMMA with a range of different injection momenta, we mimic a change in momentum by scaling the quadrupole strengths. This simulation method gives a measurement of the dynamics directly equivalent to changing the injected momentum in the whole range from 10.5 to 20.5 MeV/c. Throughout the paper, the momentum is defined in this way, and we call it 'equivalent momentum' when it has to be clearly distinguished from the real momentum.

Beam emittance measurement is available only in the beam transport line between ALICE and EMMA. Optics matching is roughly monitored by destructive yttrium aluminium garnet (YAG) screens at two locations in the ring during the injection set-up.

The orbital period is measured with a signal from one electrode of a BPM located halfway around the ring from the injection point. The circulating beam is detected and displayed on an oscilloscope for every turn. Instead of directly measuring the time difference between consecutive turns, the timing relative to the radiofrequency phase is recorded. For each equivalent momentum, the measurement was repeated eight times and is shown in Fig. 1; the momentum dependence is parabolic as predicted[16,19,31].

Because of the lattice periodicity, the BPMs lying between the two quadrupoles in each of the 42 cells should ideally record the same horizontal beam position (as a function of momentum) and a constant vertical position in the accelerator mid-plane. In reality, deviations from the ideal lattice generate observed CODs of up to ±5 mm in the horizontal and vertical planes when the fractional part of the ring tune is near 0.5. In the horizontal plane, stray fields from the injection and extraction septa have been identified as major sources of COD, but it is not known at present what is responsible in the vertical plane. The alignment of the main quadrupoles is within 0.05 mm and is thus responsible for at most ±1 mm of COD.

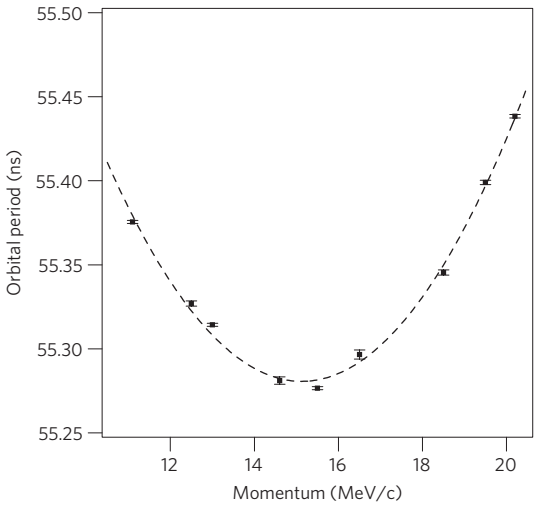

Figure 1 | Orbital period in the EMMA ring as a function of momentum, calculated from the measurement of beam arrival time over ten turns at a single BPM relative to a reference 1.3 GHz sinusoidal radiofrequency signal. The time is then scaled by the ratio of beam velocity difference between real and equivalent momenta. The error in the orbital period is the standard deviation of eight measurements. The almost quadratic behaviour of the orbital period confirms the prior theoretical prediction, and the indicated fitted second-order polynomial is used to derive a best estimate of the expected longitudinal behaviour for use in later measurements (Fig. 4).

As the phase advance in each cell is, to a good approximation, identical, the measured betatron oscillations in a portion of the ring can be used to calculate both the cell and ring tune. A numerical analysis of the fundamental frequency (NAFF) algorithm[32] was performed over twenty-one consecutive cells to obtain the fundamental frequency. The mean and standard deviation of the cell tune were calculated using the first ten turns of data and are shown in Fig. 2 along with the BPM signals.

Before attempting acceleration in a serpentine channel, which requires a high radiofrequency voltage, a lower voltage that was predicted to be insufficient to drive a serpentine channel was applied. This voltage was still sufficient to capture the injected beam within a radiofrequency bucket. There were two purposes for this initial experiment. One was to estimate the accelerating voltage per

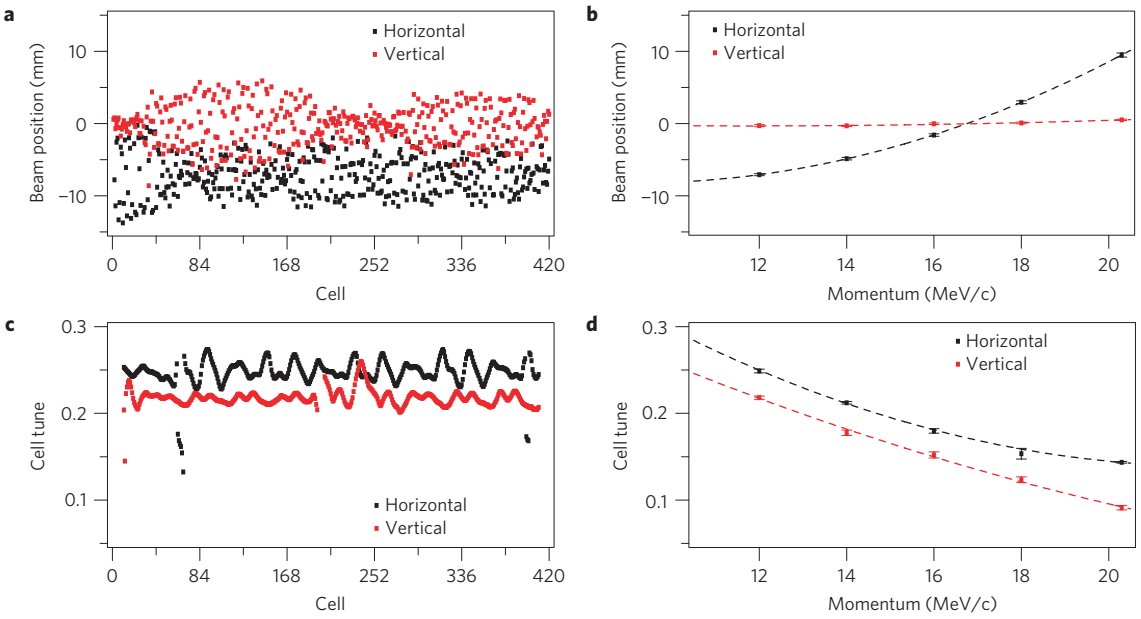

Figure 2 | Beam position and cell tune for fixed momentum beams. a, Horizontal and vertical beam position in consecutive cells over 10 turns for an equivalent momentum beam of 12.0 MeV/c. The closed orbit has small cell-to-cell fluctuations arising from magnet imperfections, around which betatron oscillations are observed. **b**, Horizontal and vertical beam position computed as an average position over 10 turns from measurements such as **a** for a range of equivalent momenta. Uncertainties shown are the standard error of the mean. **c**, Horizontal and vertical cell tune for 12.0 MeV/c equivalent momentum, computed using the NAFF (ref. 32) algorithm with a Hanning filter on horizontal and vertical position data, respectively, over a window of 21 cells centred at the indicated cell number. The value fluctuates for the same reasons as given in **a**. **d**, Horizontal and vertical tune computed as an average of tune data such as in **c**. The uncertainty reflects an upper bound estimate using the standard deviation of the data points from the average, assuming no correlation in the NAFF-estimated tunes. A least-squares fit of a second-order polynomial to the data for the horizontal position, and horizontal and vertical cell tunes are used to provide three independent mappings from measured data to momentum, which can be used to reconstruct the longitudinal phase space during acceleration (Figs 3 and 4).

turn seen by the beam; by looking at the synchrotron oscillation period in a radiofrequency bucket, the amplitude of the vector sum voltage of the cavities was estimated. The second was to measure the phase offset of the radiofrequency voltage with respect to the timing of injected beam; by scanning the radiofrequency phase from 0° to 360°, the offset value that produces the smallest synchrotron oscillations in a radiofrequency bucket was determined.

Once the radiofrequency voltage is greater than 1 MV a serpentine channel begins to appear in the longitudinal phase space; a voltage of 1.9 MV was chosen to create a wide serpentine channel. For five different initial values of the phase where serpentine channel acceleration is expected to occur, the horizontal and vertical orbit positions were measured as a function of the number of cells through which the beam has passed. The orbit and cell tune excursions, measured using consecutive BPM readings, for one case are shown in Fig. 3.

We now have all the required information to reconstruct a picture of the longitudinal phase space during acceleration. The beam momentum was extracted from previous measurements of horizontal beam position and horizontal and vertical cell tunes measured at different equivalent momenta. The phase in longitudinal phase space was derived from an independent radiofrequency phase measurement based on the BPM signal. The trajectories in longitudinal phase space were reconstructed by combining the momentum information with this phase evolution. In Fig. 4, trajectories are shown based on momenta estimated from horizontal beam position and horizontal and vertical tune.

Beam extraction is analogous to injection. The kicker pulse timing allows specific turns to be extracted following acceleration. The beam energy is measured directly after extraction using two fluorescent screens either side of the first extraction line dipole, which acts as a spectrometer. The integrated dipole field

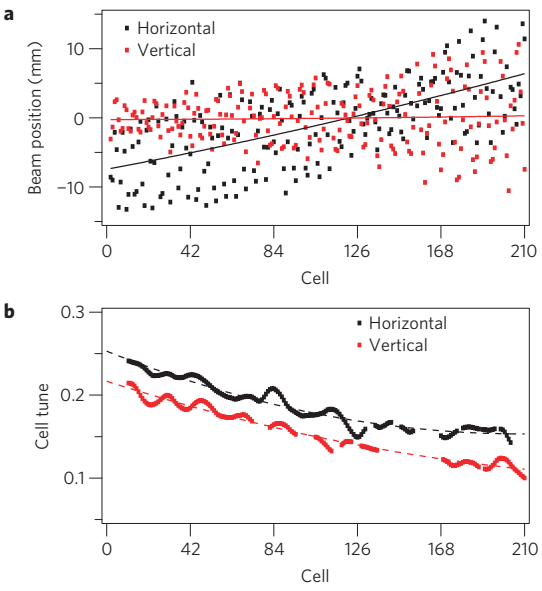

Figure 3 | Beam position and cell tune for an accelerated beam. **a**, Horizontal and vertical beam position in consecutive cells for the first five turns for a beam injected with an equivalent momentum of 12.0 MeV/c. The horizontal position shows a systematic shift due to acceleration on top of the scattered positions observed in Fig. 2a. **b**, Horizontal and vertical cell tune computed with the same method as in Fig. 2c. Both tunes show a systematic shift due to acceleration. For both results, second-order polynomial fits are performed to estimate momentum as a function of cell transited when compared to the fixed momentum data of Fig. 2b and d. This information is used in Fig. 4.

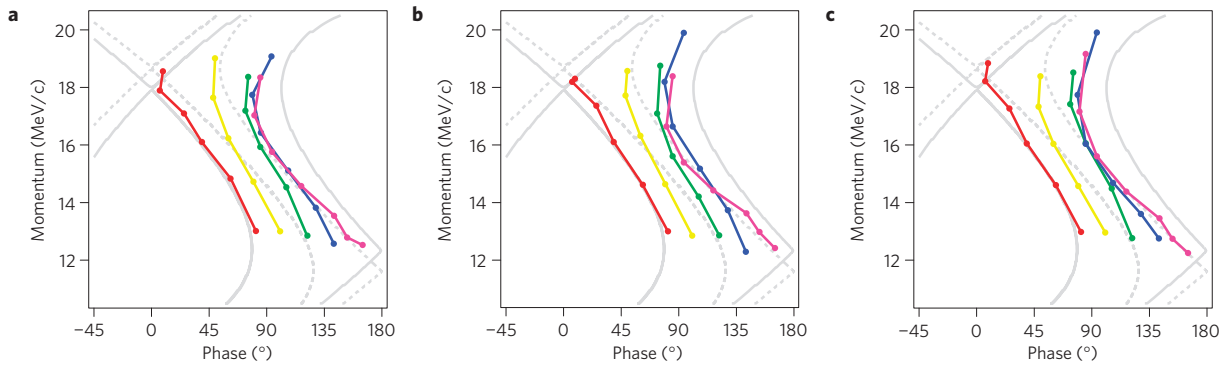

Figure 4 | Longitudinal phase space trajectories of beams with five different initial phases. All of these cases clearly demonstrate acceleration within the serpentine channel. The phase values were measured directly, whereas the momentum values were reconstructed using the polynomial fits described in Figs 2 and 3. **a**, Momentum estimated from horizontal beam position. **b**, Momentum estimated from horizontal betatron tune variation. **c**, Momentum estimated from vertical betatron tune variation. The solid and dashed grey curves indicate the best estimates of the separatrix boundary between in-bucket motion and the serpentine channel, calculated using the lower and upper bounds respectively of the estimated systematic error of ±25 ps in the orbital period measurement in Fig. 1.

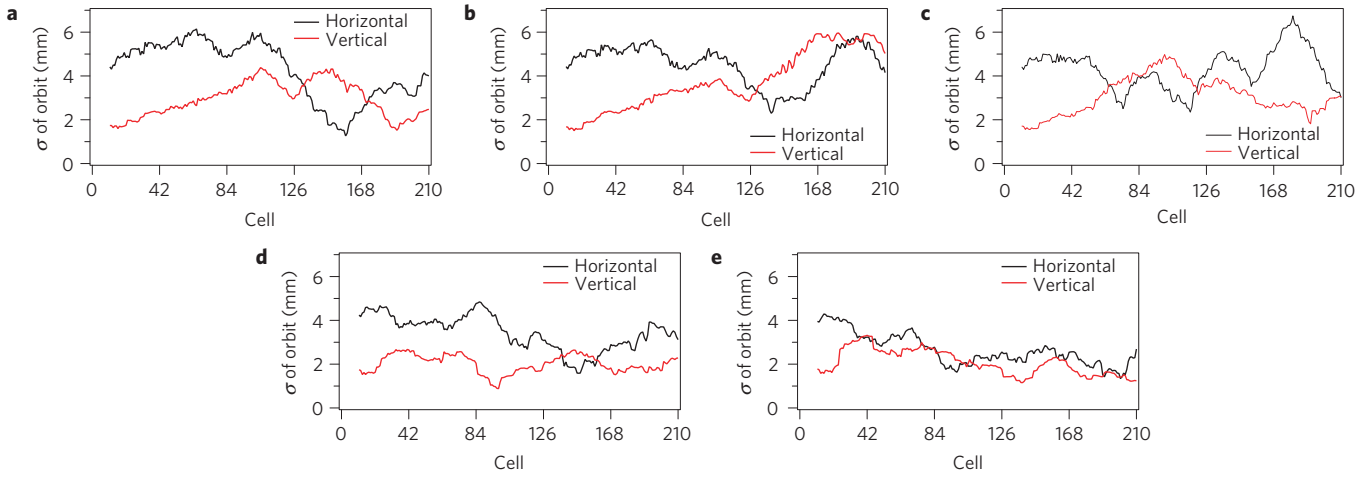

Figure 5 | Standard deviation of beam orbit oscillations in the horizontal and vertical planes, calculated at each cell using a twenty-one cell window. Results are shown for the first five turns of acceleration, for the five reconstructed trajectories in the serpentine channel in Fig. 4. **a**, Trajectory with red data, **b**, yellow data, **c**, green data, **d**, blue data, and **e**, magenta data. In all cases there is no significant growth in oscillation amplitude.

of 0.0480 T m is required to bend a beam extracted at the fifth turn by 43°, thus demonstrating acceleration from 12.5 ± 0.1 to 19.2 ± 1.0 MeV/c, corresponding to 12.0 ± 0.1 to 18.4 ± 1.0 MeV/c in equivalent momentum. The uncertainty of the extracted beam momentum is an upper bound given by the angular acceptance of the extraction line vacuum aperture.

During acceleration the cell tune changes by more than 0.1 in both horizontal and vertical planes. This implies that the total ring tune changes by more than 4.2, so that a beam must cross an integer tune a minimum of four times. In spite of this traversal of integer tunes, the BPM signals show no significant growth in beam centroid oscillation, as shown in Fig. 5.

Stable acceleration in the linear non-scaling FFAG EMMA has been successfully demonstrated. A detailed analysis further indicates that the beam is accelerated in a serpentine channel from 12.0 MeV/c to more than 18.0 MeV/c within six turns, with a small orbit shift of 10 mm. During acceleration the beam traverses several integer tunes in the horizontal and vertical planes without any observed growth in beam oscillation amplitude.

This very rapid acceleration has direct implications for the design of future muon accelerators. Furthermore, these results encourage further exploration of non-scaling FFAGs for a broad range of proton and ion accelerator applications. The practical realization of the non-scaling FFAG opens up new possibilities in the design and application of future accelerators, with the potential for widespread impact in many areas of science, technology and medicine. One example is the ongoing Particle Accelerator for MEdicaL Applications (PAMELA) project[7], which uses non-scaling FFAGs as a proton and carbon-ion source for charged-particle therapy.

Received 23 August 2011; accepted 22 November 2011; published online 10 January 2012

References

1. Symon, K. R., Kerst, D. W., Jones, L. W., Laslett, L. J. & Terwillinger, K. M. Fixed-field alternating-gradient particle accelerators. *Phys. Rev.* **103,** 1837–1859 (1956).
2. Symon, K. R. *Particle Accelerator Conference 2003* 452–456 (IEEE, 2003).
3. Machida, S. Neutrino factory design based on FFAG. *Nucl. Instrum. Methods Phys. Res. A* **503,** 41–46 (2003).
4. Keil, E. & Sessler, A. M. Muon acceleration in FFAG rings. *Nucl. Instrum. Methods Phys. Res. A* **538,** 159–177 (2005).
5. The ISS Accelerator Working Group, Apollonio, M. *et al.*. *J. Instrum.* **4,** P07001 (2009).
6. Keil, E., Sessler, A. M. & Trbojevic, D. Hadron cancer therapy complex using nonscaling fixed field alternating gradient accelerator and gantry design. *Phys. Rev. ST Accel. Beams* **10,** 054701 (2007).

7. Peach, K. *et al. International Particle Accelerator Conference 2010* 112–114 (IPAC'10 Organizing Committee, 2010).
8. Cywinski, R. *et al.* Towards a dedicated high-intensity muon facility. *Physica B* **404,** 1024–1027 (2009).
9. Tanigaki, M *et al. European Particle Accelerator Conference 2006* 2367–2369 (EPS-AG, 2006).
10. Aiba, M. *et al. European Particle Accelerator Conference 2000* 581–583 (EPS-AG, 2000).
11. Mills, F. *4th International Conference Physics Potential and Development of* $\mu^+\mu^-$ *Colliders, Transparency Book* 693–696 (UCLA, 1997).
12. Johnstone, C. *4th International Conference Physics Potential and Development of* $\mu^+\mu^-$ *Colliders, Transparency Book* 696–698 (UCLA, 1997).
13. Machida, S. & Kelliher, D. J. Orbit and optics distortion in fixed field alternating gradient muon accelerators. *Phys. Rev. ST Accel. Beams* **10,** 114001 (2007).
14. Johnstone, C., Wan, W. & Garren, A. *Particle Accelerator Conference 1999* 3068–3070 (IEEE, 1999).
15. Berg, J. S. *Snowmass 2001*, SLAC-R-599, http://www.slac.stanford.edu/econf/C010630, T503 (SLAC, 2001).
16. Johnstone, C. & Koscielniak, S. *Snowmass 2001*, SLAC-R-599, http://www.slac.stanford.edu/econf/C010630, T508 (SLAC, 2001).
17. Berg, J. S. *European Particle Accelerator Conference 2002* 1124–1126 (EPS-AG, 2002).
18. Koscielniak, S. & Johnstone, C. *Particle Accelerator Conference 2003* 1831–1833 (IEEE, 2003).
19. Johnstone, C. & Koscielniak, S. FFAGs for rapid acceleration. *Nucl. Instrum. Methods Phys. Res. A* **503,** 445–457 (2003).
20. Koscielniak, S. & Johnstone, C. Mechanisms for nonlinear acceleration in FFAGs with fixed rf. *Nucl. Instrum. Methods Phys. Res. A* **523,** 25–49 (2004).
21. Berg, J. S. Minimizing longitudinal distortion in a nearly isochronous linear nonscaling fixed-field alternating gradient accelerator. *Phys. Rev. ST Accel. Beams* **9,** 034001 (2006).
22. Machida, S. Resonance crossing and dynamic aperture in nonscaling fixed field alternating gradient accelerators. *Phys. Rev. ST Accel. Beams* **11,** 094003 (2008).
23. Keil, E. Electron model: Lattice and performance. *Nucl. Phys. B. Proc. Suppl.* **155,** 323–324 (2006).
24. Barlow, R. *et al.* EMMA—The world's first non-scaling FFAG. *Nucl. Instrum. Methods Phys. Res. A* **624,** 1–19 (2010).
25. Wheelhouse, A. *et al. International Particle Accelerator Conference 2010* 3999–4001 (IPAC'10 Organizing Committee, 2010).
26. Berg, J. S. The EMMA main ring lattice. *Nucl. Instrum. Methods Phys. Res. A* **596,** 276–284 (2008).
27. Kalinin, A., Smith, R. & McIntosh, P. A. *International Particle Accelerator Conference 2010* 1134–1136 (IPAC'10 Organizing Committee, 2011).
28. Saveliev, Y. *et al. International Particle Accelerator Conference 2010* 2350–2352 (IPAC'10 Organizing Committee, 2010).
29. Muratori, B. D., Smith, S. L., Tzenov, S. I. & Johnstone, C. *European Particle Accelerator Conference 2008* 3386–3888 (EPS-AG, 2008).
30. Smith, S. L. *19th International Conference on Cyclotrons and their Applications* 390–394 (Institute of Modern Physics (IMP), 2010).
31. Koscielniak, S. & Craddock, M. K. *European Particle Accelerator Conference 2004* 1138–1140 (EPS-AG, 2004).
32. Laskar, J., Froeschlé, C. & Celletti, A. The measure of chaos by the numerical analysis of the fundamental frequencies. Application to the standard mapping. *Physica D* **56,** 253–269 (1992).

Acknowledgements

We greatly appreciate the assistance of the Technology Department at STFC Daresbury Laboratory during the design and construction of EMMA. Our work is supported by the BASROC/CONFORM project (the UK Basic Technology Fund) under Engineering and Physical Sciences Research Council (EPSRC) Grant No. EP/E032869/1, the UK Neutrino Factory project under Particle Physics and Astronomy Research Council (PPARC) Contract No. 2054, Science and Technology Facilities Council (STFC), National Sciences and Engineering Research Council of Canada (NSERC) Grant No. SRO 328338-05 and the US Department of Energy under Contract No. DE-AC02-98CH10886 and DE-AC02-07CH11359.

Author contributions

All authors contributed extensively to the work presented in this paper.

Additional information

The authors declare no competing financial interests. Reprints and permissions information is available online at www.nature.com/reprints. Correspondence and requests for materials should be addressed to S.M.

[1]STFC Rutherford Appleton Laboratory, Harwell Oxford, Didcot, Oxon, OX11 0QX, UK, [2]University of Huddersfield, Huddersfield, HD1 3DH, UK, [3]Brookhaven National Laboratory, Upton, New York 11973-5000, USA, [4]STFC Daresbury Laboratory, Warrington, Cheshire, WA4 4AD, UK, [5]Cockcroft Institute of Accelerator Science and Technology, Daresbury, Warrington, WA4 4AD, UK, [6]TRIUMF, Vancouver, British Columbia V6T 2A3, Canada, [7]University of British Columbia, Vancouver, British Columbia V6T 1Z1, Canada, [8]University College London, London, WC1E 6BT, UK, [9]University of Manchester, Manchester, M13 9PL, UK, [10]Brunel University, Uxbridge, Middlesex, UB8 3PH, UK, [11]Australian Synchrotron, Clayton, Victoria 3168, Australia, [12]University of Liverpool, Liverpool, L69 7ZE, UK, [13]Fermi National Accelerator Laboratory, Batavia, Illinois 60510-5011, USA, [14]CERN, Geneva, CH-1211, Switzerland, [15]Imperial College London, London, SW7 2AZ, UK, [16]John Adams Institute for Accelerator Science, University of Oxford, OX1 3RH, UK, [17]Lancaster University, Lancaster, LA1 4YW, UK. *e-mail: shinji.machida@stfc.ac.uk.